ACS Energy LETTERS

http://pubs.acs.org/journal/aelccp

LETTER

Light-Harvesting "Antenna" Behavior in NU-1000

Subhadip Goswami, Jierui Yu, Sameer Patwardhan, Pravas Deria,* and Joseph T. Hupp*

Cite This: *ACS Energy Lett.* 2021, 6, 848–853

Read Online

ACCESS | Metrics & More | Article Recommendations | Supporting Information

ABSTRACT: Structural or conceptual synthetic analogues of natural photosynthetic light-harvesting complexes hold promise as entities capable of both efficient collection of visible-region solar photons and rapid and efficient delivery of stored solar energy to energy-converting electrodes or chemical catalysts. Porous, crystalline metal−organic frameworks (MOFs) are promising supramolecular scaffolds for this purpose. Here, we report on the "antenna behavior" of chromophore assemblies comprising aligned organic linkers within a zirconium-based MOF, NU-1000. The behavior was probed primarily via amplified emission quenching using either an electron donor (ferrocene carboxylate) or an electron acceptor (3,5-dinitrobenzoate) as a redox quencher. We used solvent-assisted ligand incorporation (SALI) as a versatile means of siting/immobilizing desired quencher molecules directly within the extended chromophoric structures. We find that a photogenerated molecular exciton (spanning about four linkers) can sample ∼300 chromophoric linkers—behavior which translates to a single-step energy-transfer or exciton-hopping time of a few picoseconds. These findings clearly suggest that NU-1000 and similar MOFs can offer an "antenna" of significant size and that with a suitable catalyst immobilized on the MOF node, can find application in solar energy conversion devices.

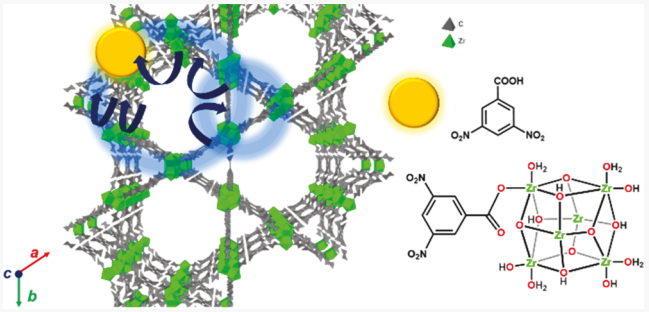

The chlorophyll special pair in the photosynthetic apparatus of plants absorbs light and then uses the briefly stored energy to initiate charge transfer, culminating either in water oxidation to O_2 (photosystem II) or in formation of carbohydrates from CO_2 (photosystem I).[1] Special pairs are strongly chromophoric; nevertheless, the overwhelming majority of photons driving photosynthesis are collected not by the special pair, but by self-assembled and protein-assembled arrays of chlorophyll *b* and other pigments. Rapid Förster-like resonance energy transfer (FRET) serves to channel remotely captured photonic energy through the arrays and to the special pair, which can then initiate chemistry in the same way as if the pair had directly absorbed photons.

Key to fast energy transfer is optimal spacing, alignment, and relative orientation of energy donors and energy acceptors, together with precise energy matching as indicated by high overlap of donor emission and acceptor absorption spectra. We and others have pursued the idea that appropriately designed metal−organic frameworks (MOFs) can function as artificial light-harvesting arrays and as antennae for transporting remotely collected energy to a site proximal to an energy-converting catalyst, redox shuttle, or electrode.[2−16]

The attractions of MOFs for these kinds of studies include their crystalline periodicity, molecular-scale porosity, and broad structural, topological, and compositional tunability,[17] Consisting of inorganic nodes and organic linkers,[18] MOFs can most easily be rendered chromophoric by choosing molecular chromophores themselves as linkers—typically in combination with redox-inert nodes if retaining linker luminescence is important. Suitably chosen MOFs can be readily integrated with electrodes and permeated with solvent, rendering them functional for electrocatalytic,[19−22] electroanalytical,[23−25] or photoelectrochemical applications.[26] Finally, many MOFs featuring metal-oxo clusters rather than individual metal ions or pairs of metal ions as nodes, devote only a fraction of potential coordination sites to linker binding. The remaining sites can be used to graft catalysts, redox shuttles, or auxiliary chromophores—with the grafted moieties themselves now being periodically arrayed within a porous framework.

Herein we report on linker-based energy transfer within NU-1000, a near-UV and blue-absorbing MOF that exhibits the

Received: December 2, 2020
Accepted: January 29, 2021
Published: February 5, 2021

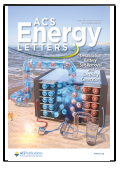

https://dx.doi.org/10.1021/acsenergylett.0c02514
ACS Energy Lett. 2021, 6, 848–853

aforementioned characteristics.[27] A portion of the semi-infinite crystalline structure of NU-1000 is shown in Figure 1. The

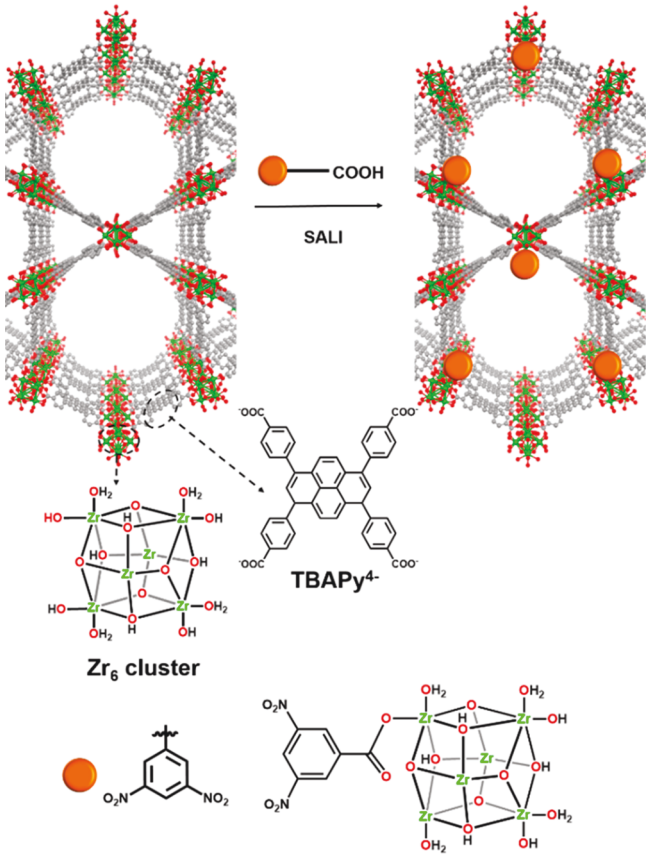

Figure 1. Solvent-assisted ligand incorporation (SALI) of NU-1000 with 3,5-dinitrobenzoic acid.

question we seek to answer is the extent to which the MOF can function as a light-harvesting antenna for delivering oxidizing or reducing equivalents to remotely sited molecular quenchers. Expressed more simply, we seek to determine experimentally how many linkers a photogenerated molecular exciton can visit in its brief singlet excited-state lifetime. (NU-1000 holds special interest because of recent theoretical and experimental work indicating that relevant singlet excited states are delocalized over four, or possibly more, tetraphenyl-carboxylate-pyrene ($TBAPy^{4-}$) linkers.[28])

We deduced the number of linkers visited by randomly doping NU-1000 with varying (known) amounts of a redox quencher, and then monitoring and assessing the ensuing decreases in fluorescence intensity and excited-state lifetime. Previously it has been shown that by utilizing solvent-assisted ligand incorporation (SALI), free-base porphyrin and ferrocene can be grafted to the nodes of NU-1000;[29−33] photoluminescence from NU-1000 is quenched by energy and electron transfer (free-base porphyrin/Zn-metalated porphyrin),[30] or by hole transfer (ferrocene).[34] Here, we similarly graft a well-known electron acceptor, 3,5-dinitrobenzoate (DNB),[35] to the Zr_6 nodes of NU-1000.[36,37] (See Supporting Information (SI) for details of DNB installation and quantification of DNB loading.)

Diffuse reflectance infrared Fourier transform (DRIFT) spectra were recorded to verify binding of the carboxy-appended DNB ligand to the Zr_6 node and provide insight into the mode of binding (Figures S8 and S9).[38] The $Zr_6(\mu_3\text{-}O)_4(\mu_3\text{-}OH)_4$ nodes of benzoate-free NU-1000 (obtained by heating the as-synthesized MOF aqueous HCl/DMF) are known to coordinate, in addition to eight bidentate carboxylates from linkers, a combination of adventitious formate (also bound in bidentate fashion) and hydrogen-bonded terminal aqua/hydroxo pairs. The bridging and terminal hydroxos together yield a sharp peak—an O−H stretch—at 3674 cm^{-1}, while aqua ligands contribute a shoulder at 3672 cm^{-1}.[39] Monodentate carboxy-binding of a DNB[32] in place of a terminal hydroxo ligand serves to maintain charge-balance, while leaving a terminal aqua ligand in place; consequently, the relative intensity of the 3672 cm^{-1} peak increases, as evidenced most clearly for high-loading samples, i.e. samples containing 1.4 DNB ligands per node. For lower loading (e.g., 0.01-DNB-NU-1000), however, the increase in relative intensity evidently is too small to observe.

As shown in Figure 2, panels A and B, substantial quenching of steady-state fluorescence accompanies the introduction of

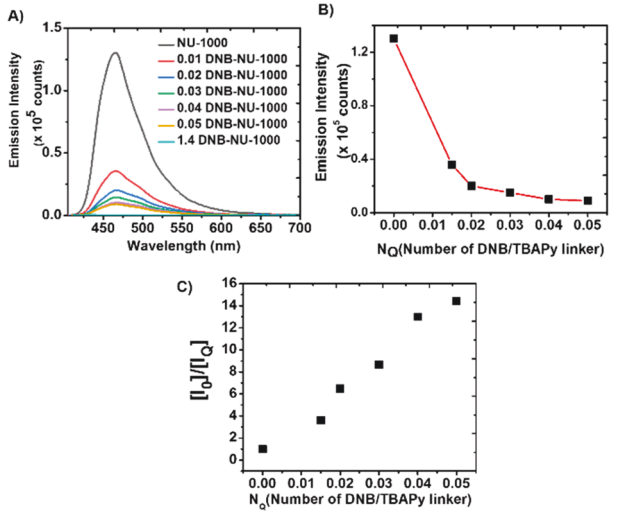

Figure 2. (A) Steady-state fluorescence spectra of pristine NU-1000 and the DNB-containing samples in 2-MeTHF. (B) Variation of fluorescence intensity with respect to the number of quencher molecules (N_Q) per TBAPy linker. (C) Stern−Volmer-like plot obtained by plotting I_0/I_Q vs N_Q.

even small amounts of node-grafted DNB. Indeed, quenching is more than 50% complete when the number of DNB molecules per TBAPy linker, N_Q, is 0.01, and more than 90% complete when N_Q = 0.04. This behavior is a signature of "antenna-like" light-harvesting and exciton delivery.[40−42] To quantify the quenching, and associated linker-to-linker energy transfer phenomenon, we turned to the following Stern−Volmer-like equation:[7,43]

$$\frac{I_0}{I_Q} = 1 + K_{SV}N_Q \quad (1)$$

In eq 1, I_0 is the fluorescence intensity in absence of quencher, I_Q is the fluorescence intensity in the presence of a particular amount of quencher, K_{SV} is the Stern−Volmer quenching constant, and N_Q is defined above. In contrast to energy transfer in homogeneous solution, where the quencher diffuses to the chromophore, here the quencher is immobilized, as are the chromophoric linkers. Instead, the diffusing entity is molecular exciton. Importantly, K_{SV} can be replaced by N_t

https://dx.doi.org/10.1021/acsenergylett.0c02514
ACS Energy Lett. 2021, 6, 848−853

(number of chromophores the exciton visits within its lifetime); nevertheless, it is still expressed as $\tau_0\ k_e$.

Fits of plots (Figure 2C) with eq 1 indicate that the exciton can sample ~270 linkers in its lifetime. A similar plot for ferrocene carboxylate (Fc) as a quencher (Figure 3A,B) shows

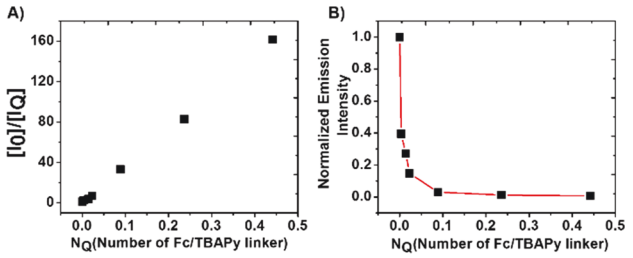

Figure 3. (A) Stern−Volmer-like plot of I_0/I_Q vs N_Q. (B) Variation of normalized fluorescence intensity with respect to the number of quencher molecules (N_Q) per TBAPy linker when ferrocene was used as a quencher.

the exciton can sample ~360 linkers. If quenching is rapid relative to the exciton lifetime, we would ideally expect, for the oxidative and reductive pathways, identical values for N_t. With that in mind, we will use the average of the two values going forward, $N_t = 315 \pm 45$.

As exciton hopping is a diffusional process, statistically, each successive hop can take the exciton one step closer to or one step away from the source. If, for simplicity, we consider the diffusive transport to be 1-dimensional, and we treat the exciton as if it is localized on a single linker, the total number of hops an exciton would make in sampling 315 linkers is, on average, ~12 400 ($= 315^2/8$). Time-resolved fluorescence measurements show that, in the absence of quenchers, the major component of the emission decay, τ_0, is 1.2 ns—implying a single-step hopping time of ~100 fs ($= \tau_0/12\,400$). If correct, exciton hopping in NU-1000 would be ~30−50 times faster than is typical for hopping in natural light-harvesting complexes.[44,45]

Note, however, that excitons in NU-1000 are delocalized over several linkers/chromophores.[28] As such, each hop can be expected to sample multiple new linkers, the number of hops required is much less and the single-step energy-transfer time is much longer. For example, if the exciton is delocalized over 4 linkers, and the number of new linkers sampled with each hop is likewise 4, the number of hops accomplished during the brief lifetime of the exciton would be $12\,400/4^2 \approx 800$, and the hopping time would be ~1.5 ps. Similarly, if the exciton were delocalized over, say, nine linkers, the number of hops and hopping time would be ~150 and ~8 ps, respectively.

Finally, the available time-resolved fluorescence quenching data (e.g., decay curves in Figure 4), together with measures of absolute quantum yield (φ), can be used to estimate rates of charge transfer between quenchers and immediately proximal NU-1000* excitons. The absolute quantum yield of the samples decreases with an increasing amount of quencher from 51% to 0.1% (Table S2).[46] Similar to I_0/I_Q, we can plot φ_0/φ_Q vs DNB/TBAPy linker to obtain the saturated quantum yield in the presence of quencher (not shown here). With the increasing addition of the quencher, the fluorescence lifetime shows a concomitant decrease (Figure 4). The major fast component of the lifetime decreased from 1.2 to 0.03 ns. From the saturated emission quenching and the corresponding

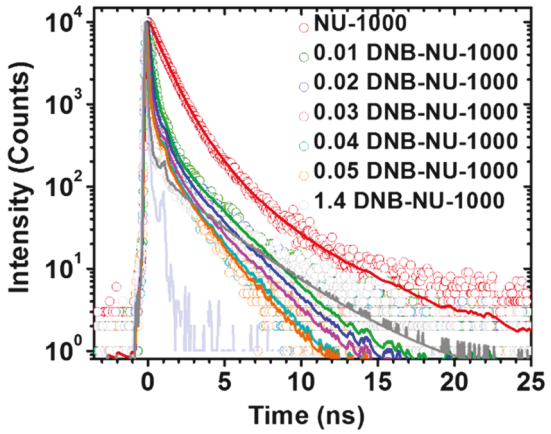

Figure 4. Transient emission decay profiles of NU-1000 and DNB-NU-1000 samples, highlighting the faster decay kinetics with increasing DNB amount within NU-1000.

lifetime data, we can obtain the rate of electron transfer (from NU-1000* to DNB) via

$$\frac{I_0}{I_S} = \frac{\varphi_0}{\varphi_S} = 1 + \tau_0 k_e \tag{2}$$

where I_0, φ_0, and τ_0 are the intrinsic fluorescence intensity, quantum yield, and lifetime, respectively. I_S and φ_S are the saturated fluorescence intensity and quantum yield in the presence of quencher Q, respectively. k_e is the first-order electron-transfer rate constant and is estimated to be 1.1×10^{10} s^{-1}.[47] An order of magnitude faster rate of hole transfer is observed (~10^{11} s^{-1}) from NU-1000* to Fc in Fc-NU-1000.

To estimate the thermodynamic driving force for electron transfer from NU-1000* to DNB, we employed the following Rehm−Weller expression:[48]

$$\Delta G^0 = e(E^{D}_{Ox} - E^{A}_{Red}) - \Delta E_{0,0} - \frac{e^2}{4\pi\epsilon_0\epsilon_s R_{DA}} - \frac{e^2}{8\pi\epsilon_0}\left(\frac{1}{r_D} - \frac{1}{r_A}\right)\left(\frac{1}{\epsilon_{ref}} - \frac{1}{\epsilon_s}\right) \tag{3}$$

In eq 3, e is the unit electronic charge, E^{D}_{Ox} and E^{A}_{Red} are the electrochemically determined formal potentials of NU-1000 (1.35 V (vs Ag/AgCl); the potential for one-electron reduction of the pyrene-radical-cation-containing linker, i.e., the oxidized linker)[34] and DNB (−0.68 V; the potential for one-electron reduction of DNB to its radical anion form).[49] $\Delta E_{0,0}$ is the excitation energy of NU-1000 and is estimated as ~3.2 eV. The remaining terms account for electrostatic interactions, where r_D and r_A are the effective radii of the donor TBAPy (7.4 Å) and the acceptor DNB (3.7 Å), respectively. The effective center-to-center distance (8.8 Å) between donor and acceptor (R_{DA}) is estimated from the DFT optimized structure (see Figure 6; for computational details, see Supporting Information section S4).[50] ϵ_0 is the permittivity of free space, ϵ_s is the static dielectric constant of the solvent MeTHF, and ϵ_{ref} is the dielectric constant of the solvent (DCM) in which the electrochemical potentials were measured. As illustrated in Figure 5, photoexcited NU-1000 is a strong reductant (E = −1.75 V) and the thermodynamic driving force, ΔG^0, for electron transfer from NU-1000* to DNB is −1.4 eV. For comparison, the driving force for hole transfer from photo-excited NU-1000 to node-ligated ferrocene (or electron

https://dx.doi.org/10.1021/acsenergylett.0c02514
ACS Energy Lett. 2021, 6, 848−853

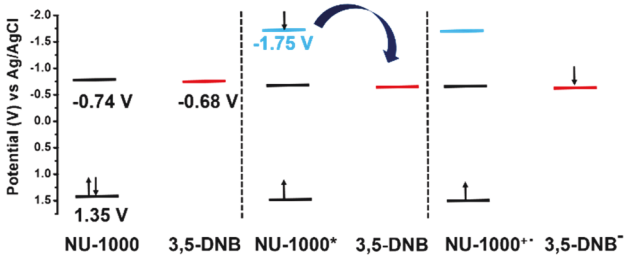

Figure 5. Diagrams relevant to energetics of redox quenching of NU-1000* (i.e., photoexcited NU-1000). Left: electrochemically determined redox potentials for NU-1000$^{+/0}$, NU-1000$^{0/-}$ (black), and 3,5-DNB$^{0/-}$ (red). Center: NU-1000*$^{/+}$ redox potential (cyan). Labels along the bottom indicate electron distribution before photoexcitation (left), after photoexcited state generation (center), and after oxidative redox quenching of photoexcited NU-1000 by DNB. The disparity between the reducing strength of electrogenerated NU-1000^{-} and photogenerated NU-1000* has been discussed by Yu et al. (see ref 28).

transfer from Fc to NU-1000*) is only about −0.8 eV,[34,51] yet the charge-transfer rate is faster.

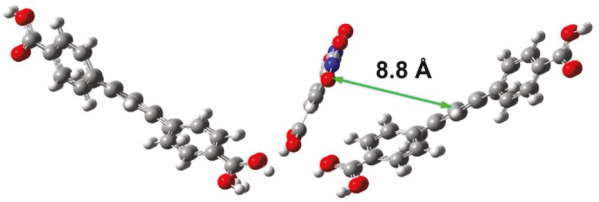

Figure 6. DFT-optimized geometry of DNB with respect to TBAPy linkers in NU-1000.

To understand the rate behavior, we turned to Marcus theory, where the first-order rate constant for electron/hole transfer in a weakly coupled system (such as a linker-excited MOF in combination with a node-tethered guest) can be described by

$$k_{e/h} = \frac{2\pi}{\hbar} H_{DA}^2 \frac{1}{\sqrt{4\pi\lambda_t k_B T}} \exp\left[-\frac{(\lambda_t + \Delta G^0)^2}{4\pi\lambda_t k_B T}\right] \quad (4)$$

Here, H_{DA} represents the strength of electronic coupling between the donor and acceptor; λ_t is the total reorganization energy comprising λ_i, the internal reorganization energy due to displacement of atomic nuclei along vibrational coordinates for reactants vs products, λ_s the solvent reorganization energy; k_B is the Boltzmann constant. Notably, in the absence of a superior through-bond pathway, H_{DA} increases with decreasing donor−acceptor separation distance, while λ_s decreases. The upper limit of applicability of eq 4 is reached when electronic coupling cedes control of the dynamics of charge transfer to nuclear motion. In this limit, under barrierless conditions, $\lambda_t = -\Delta G$, and $k_{e/h}$ peaks at $\sim 10^{13}$ s^{-1}.

The rate constants observed here are within 2−3 orders of magnitude of this maximum, suggesting that λ_t in both instances is within a few tenths of an eV of $-\Delta G$. Given the large gulf in values for $-\Delta G$, the most economical interpretation is that electron transfer from Fc to NU-1000* occurs in the Marcus normal or barrierless region ($\lambda_t \leq -\Delta G$) and electron transfer from NU-1000* to DNB occurs in the Marcus inverted region.

In summary, we find that the mesoporous zirconium-based MOF, NU-1000, can function as a light-harvesting antenna for delivery of absorbed energy to remotely sited electron donors or acceptors. The antenna comprises ∼300 framework linkers and energy is propagated via FRET. The corresponding excitons are delocalized over multiple linkers, thereby enabling energy to be moved by four or more linkers per exciton-hopping step. On the order of 800 hops are executed by the photogenerated exciton during its brief lifetime. The time required for a single hop is estimated to be a few picoseconds.

Excitonic energy transport culminates in either electron-transfer from NU-1000* to node-grafted DNB or hole-transfer to similarly grafted Fc, with first-order charge-transfer rate constants of $\sim 1 \times 10^{10}$ and 1×10^{11} s^{-1}, respectively. Despite the kinetic similarity, the thermodynamic driving forces for the two reactions differ by ∼0.6 eV. We suggest that redox quenching by DNB occurs in the Marcus inverted region, with quenching by Fc occurring in either the Marcus normal region or the barrierless region.

The combined results point to the potential for chromophoric MOFs to be used as artificial light-harvesting complexes in applications centering on light-to-electrical energy conversion or catalyst-facilitated, light-to-chemical energy conversion.

Identification scheme for NU-1000:[52] MOF-key, Zr.HVCDAMXLLUJLQZ.MOFkey-v1.csq; MOF-ID, O[Zr]-123([OH2])[OH]4[Zr]56[O]3[Zr]37([OH]2[Zr]28[O]1-[Zr]14([O]6[Zr]([OH]53)([OH]21)([O]78)([OH2])O)-([OH2])O)([OH2])O.[O-]C(=O)c1ccc(cc1)c1cm3(c2ccc-(cc2)C(=O)[O-])c2c3c1ccc1c3c(cc2)c(cc1c1ccc(cc1)C(=O)[O-])c1ccc(cc1)C(=O)[O-] MOFid-v1.csq.cat0.

■ ASSOCIATED CONTENT

Supporting Information

The Supporting Information is available free of charge at https://pubs.acs.org/doi/10.1021/acsenergylett.0c02514.

Experimental details, including instrumentation and synthesis, and computational details; Figures S1−S7, NMR spectra; Figures S8 and S9, DRIFTS spectra; Figure S10, PXRD patterns; Table S1, time-resolved emission data; Figure S11, Stern−Volmer-like plot of t_0/t_Z vs N_Q; Figure S12 SEM pictures and EDS spectrum; and Table S2, fluorescence quantum yield of NU-1000 and X-DNB-NU-1000 (PDF)

■ AUTHOR INFORMATION

Corresponding Authors

Pravas Deria − *Department of Chemistry and Biochemistry, Southern Illinois University, Carbondale, Illinois 62901, United States;* orcid.org/0000-0001-7998-4492; Email: pderia@siu.edu

Joseph T. Hupp − *Department of Chemistry, Northwestern University, Evanston, Illinois 60208, United States;* orcid.org/0000-0003-3982-9812; Email: j-hupp@northwestern.edu

Authors

Subhadip Goswami − *Department of Chemistry, Northwestern University, Evanston, Illinois 60208, United States;* orcid.org/0000-0002-8462-9054

https://dx.doi.org/10.1021/acsenergylett.0c02514
ACS Energy Lett. 2021, 6, 848−853

Jierui Yu − *Department of Chemistry and Biochemistry, Southern Illinois University, Carbondale, Illinois 62901, United States;* orcid.org/0000-0001-8422-3583
Sameer Patwardhan − *Department of Chemistry, Northwestern University, Evanston, Illinois 60208, United States;* orcid.org/0000-0001-9118-8018

Complete contact information is available at: https://pubs.acs.org/10.1021/acsenergylett.0c02514

Notes

The authors declare no competing financial interest.

■ ACKNOWLEDGMENTS

For work done at Northwestern, we gratefully acknowledge support from the U.S. Department of Energy, Office of Science, Office of Basic Energy Sciences via grant DE-FG02-87ER13808. P.D. acknowledges funding from the U.S. National Science Foundation (NSF CAREER CHE-1944903). This work made use of the IMSERC facility at Northwestern University, which has received support from the NSF (CHE-1048773 and DMR-0521267); SHyNE Resource (NSF NNCI-1542205); and the State of Illinois and IIN.

■ REFERENCES

(1) Scholes, G. D.; Fleming, G. R.; Olaya-Castro, A.; van Grondelle, R. Lessons from nature about solar light harvesting. *Nat. Chem.* **2011**, *3* (10), 763−774.
(2) Goswami, S.; Chen, M.; Wasielewski, M. R.; Farha, O. K.; Hupp, J. T. Boosting Transport Distances for Molecular Excitons within Photoexcited Metal−Organic Framework Films. *ACS Appl. Mater. Interfaces* **2018**, *10* (40), 34409−34417.
(3) Goswami, S.; Ma, L.; Martinson, A. B. F.; Wasielewski, M. R.; Farha, O. K.; Hupp, J. T. Toward Metal−Organic Framework-Based Solar Cells: Enhancing Directional Exciton Transport by Collapsing Three-Dimensional Film Structures. *ACS Appl. Mater. Interfaces* **2016**, *8* (45), 30863−30870.
(4) Spoerke, E. D.; Small, L. J.; Foster, M. E.; Wheeler, J.; Ullman, A. M.; Stavila, V.; Rodriguez, M.; Allendorf, M. D. MOF-Sensitized Solar Cells Enabled by a Pillared Porphyrin Framework. *J. Phys. Chem. C* **2017**, *121* (9), 4816−4824.
(5) Zhu, J.; Maza, W. A.; Morris, A. J. Light-harvesting and energy transfer in ruthenium(II)-polypyridyl doped zirconium(IV) metal-organic frameworks: A look toward solar cell applications. *J. Photochem. Photobiol., A* **2017**, *344*, 64−77.
(6) Kent, C. A.; Liu, D.; Ma, L.; Papanikolas, J. M.; Meyer, T. J.; Lin, W. Light Harvesting in Microscale Metal−Organic Frameworks by Energy Migration and Interfacial Electron Transfer Quenching. *J. Am. Chem. Soc.* **2011**, *133* (33), 12940−12943.
(7) Son, H.-J.; Jin, S.; Patwardhan, S.; Wezenberg, S. J.; Jeong, N. C.; So, M.; Wilmer, C. E.; Sarjeant, A. A.; Schatz, G. C.; Snurr, R. Q.; Farha, O. K.; Wiederrecht, G. P.; Hupp, J. T. Light-Harvesting and Ultrafast Energy Migration in Porphyrin-Based Metal−Organic Frameworks. *J. Am. Chem. Soc.* **2013**, *135* (2), 862−869.
(8) Williams, D. E.; Rietman, J. A.; Maier, J. M.; Tan, R.; Greytak, A. B.; Smith, M. D.; Krause, J. A.; Shustova, N. B. Energy Transfer on Demand: Photoswitch-Directed Behavior of Metal−Porphyrin Frameworks. *J. Am. Chem. Soc.* **2014**, *136* (34), 11886−11889.
(9) Deria, P.; Yu, J.; Balaraman, R. P.; Mashni, J.; White, S. N. Topology-dependent emissive properties of zirconium-based porphyrin MOFs. *Chem. Commun.* **2016**, *52* (88), 13031−13034.
(10) Yu, J.; Anderson, R.; Li, X.; Xu, W.; Goswami, S.; Rajasree, S. S.; Maindan, K.; Gómez-Gualdrón, D. A.; Deria, P. Improving Energy Transfer within Metal−Organic Frameworks by Aligning Linker Transition Dipoles along the Framework Axis. *J. Am. Chem. Soc.* **2020**, *142* (25), 11192−11202.
(11) Shaikh, S. M.; Chakraborty, A.; Alatis, J.; Cai, M.; Danilov, E.; Morris, A. J. Light harvesting and energy transfer in a porphyrin-based metal organic framework. *Faraday Discuss.* **2019**, *216*, 174−190.
(12) Maza, W. A.; Padilla, R.; Morris, A. J. Concentration Dependent Dimensionality of Resonance Energy Transfer in a Postsynthetically Doped Morphologically Homologous Analogue of UiO-67 MOF with a Ruthenium(II) Polypyridyl Complex. *J. Am. Chem. Soc.* **2015**, *137* (25), 8161−8168.
(13) Haldar, R.; Heinke, L.; Wöll, C. Advanced Photoresponsive Materials Using the Metal−Organic Framework Approach. *Adv. Mater.* **2020**, *32* (20), 1905227.
(14) Martin, C. R.; Kittikhunnatham, P.; Leith, G. A.; Berseneva, A. A.; Park, K. C.; Greytak, A. B.; Shustova, N. B. Let the light be a guide: Chromophore communication in metal-organic frameworks. *Nano Res.* **2021**, *14* (2), 338−354.
(15) Rice, A. M.; Martin, C. R.; Galitskiy, V. A.; Berseneva, A. A.; Leith, G. A.; Shustova, N. B. Photophysics Modulation in Photoswitchable Metal−Organic Frameworks. *Chem. Rev.* **2020**, *120* (16), 8790−8813.
(16) Lu, J.; Pattengale, B.; Liu, Q.; Yang, S.; Shi, W.; Li, S.; Huang, J.; Zhang, J. Donor−Acceptor Fluorophores for Energy-Transfer-Mediated Photocatalysis. *J. Am. Chem. Soc.* **2018**, *140* (42), 13719−13725.
(17) Lu, W.; Wei, Z.; Gu, Z.-Y.; Liu, T.-F.; Park, J.; Park, J.; Tian, J.; Zhang, M.; Zhang, Q.; Gentle, T., III; Bosch, M.; Zhou, H.-C. Tuning the structure and function of metal−organic frameworks via linker design. *Chem. Soc. Rev.* **2014**, *43* (16), 5561−5593.
(18) Furukawa, H.; Cordova, K. E.; O'Keeffe, M.; Yaghi, O. M. The Chemistry and Applications of Metal-Organic Frameworks. *Science* **2013**, *341* (6149), 1230444.
(19) Hod, I.; Sampson, M. D.; Deria, P.; Kubiak, C. P.; Farha, O. K.; Hupp, J. T. Fe-Porphyrin-Based Metal−Organic Framework Films as High-Surface Concentration, Heterogeneous Catalysts for Electrochemical Reduction of CO2. *ACS Catal.* **2015**, *5* (11), 6302−6309.
(20) Wang, H.-F.; Chen, L.; Pang, H.; Kaskel, S.; Xu, Q. MOF-derived electrocatalysts for oxygen reduction, oxygen evolution and hydrogen evolution reactions. *Chem. Soc. Rev.* **2020**, *49* (5), 1414−1448.
(21) Miner, E. M.; Dincă, M. Metal-organic frameworks: Evolved oxygen evolution catalysts. *Nat. Energy* **2016**, *1* (12), 16186.
(22) Downes, C. A.; Marinescu, S. C. Electrocatalytic Metal−Organic Frameworks for Energy Applications. *ChemSusChem* **2017**, *10* (22), 4374−4392.
(23) Goswami, S.; Hod, I.; Duan, J. D.; Kung, C.-W.; Rimoldi, M.; Malliakas, C. D.; Palmer, R. H.; Farha, O. K.; Hupp, J. T. Anisotropic Redox Conductivity within a Metal−Organic Framework Material. *J. Am. Chem. Soc.* **2019**, *141* (44), 17696−17702.
(24) Maindan, K.; Li, X.; Yu, J.; Deria, P. Controlling Charge-Transport in Metal−Organic Frameworks: Contribution of Topological and Spin-State Variation on the Iron−Porphyrin Centered Redox Hopping Rate. *J. Phys. Chem. B* **2019**, *123* (41), 8814−8822.
(25) Mancuso, J. L.; Mroz, A. M.; Le, K. N.; Hendon, C. H. Electronic Structure Modeling of Metal−Organic Frameworks. *Chem. Rev.* **2020**, *120* (16), 8641−8715.
(26) Deng, X.; Li, R.; Wu, S.; Wang, L.; Hu, J.; Ma, J.; Jiang, W.; Zhang, N.; Zheng, X.; Gao, C.; Wang, L.; Zhang, Q.; Zhu, J.; Xiong, Y. Metal−Organic Framework Coating Enhances the Performance of Cu2O in Photoelectrochemical CO2 Reduction. *J. Am. Chem. Soc.* **2019**, *141* (27), 10924−10929.
(27) Mondloch, J. E.; Bury, W.; Fairen-Jimenez, D.; Kwon, S.; DeMarco, E. J.; Weston, M. H.; Sarjeant, A. A.; Nguyen, S. T.; Stair, P. C.; Snurr, R. Q.; Farha, O. K.; Hupp, J. T. Vapor-Phase Metalation by Atomic Layer Deposition in a Metal−Organic Framework. *J. Am. Chem. Soc.* **2013**, *135* (28), 10294−10297.
(28) Yu, J.; Park, J.; Van Wyk, A.; Rumbles, G.; Deria, P. Excited-State Electronic Properties in Zr-Based Metal−Organic Frameworks as a Function of a Topological Network. *J. Am. Chem. Soc.* **2018**, *140* (33), 10488−10496.

(29) Deria, P.; Bury, W.; Hupp, J. T.; Farha, O. K. Versatile functionalization of the NU-1000 platform by solvent-assisted ligand incorporation. *Chem. Commun.* **2014**, *50* (16), 1965−1968.
(30) Li, X.; Yu, J.; Gosztola, D. J.; Fry, H. C.; Deria, P. Wavelength-Dependent Energy and Charge Transfer in MOF: A Step toward Artificial Porous Light-Harvesting System. *J. Am. Chem. Soc.* **2019**, *141* (42), 16849−16857.
(31) Hod, I.; Bury, W.; Gardner, D. M.; Deria, P.; Roznyatovskiy, V.; Wasielewski, M. R.; Farha, O. K.; Hupp, J. T. Bias-Switchable Permselectivity and Redox Catalytic Activity of a Ferrocene-Functionalized, Thin-Film Metal−Organic Framework Compound. *J. Phys. Chem. Lett.* **2015**, *6* (4), 586−591.
(32) Liu, J.; Li, Z.; Zhang, X.; Otake, K.-i.; Zhang, L.; Peters, A. W.; Young, M. J.; Bedford, N. M.; Letourneau, S. P.; Mandia, D. J.; Elam, J. W.; Farha, O. K.; Hupp, J. T. Introducing Nonstructural Ligands to Zirconia-like Metal−Organic Framework Nodes To Tune the Activity of Node-Supported Nickel Catalysts for Ethylene Hydrogenation. *ACS Catal.* **2019**, *9* (4), 3198−3207.
(33) Goswami, S.; Noh, H.; Redfern, L. R.; Otake, K.-i.; Kung, C.-W.; Cui, Y.; Chapman, K. W.; Farha, O. K.; Hupp, J. T. Pore-Templated Growth of Catalytically Active Gold Nanoparticles within a Metal−Organic Framework. *Chem. Mater.* **2019**, *31* (5), 1485−1490.
(34) Van Wyk, A.; Smith, T.; Park, J.; Deria, P. Charge-Transfer within Zr-Based Metal−Organic Framework: The Role of Polar Node. *J. Am. Chem. Soc.* **2018**, *140* (8), 2756−2760.
(35) Lambrev, P. H.; Schmitt, F.-J.; Kussin, S.; Schoengen, M.; Várkonyi, Z.; Eichler, H. J.; Garab, G.; Renger, G. Functional domain size in aggregates of light-harvesting complex II and thylakoid membranes. *Biochim. Biophys. Acta, Bioenerg.* **2011**, *1807* (9), 1022−1031.
(36) Webber, T. E.; Liu, W.-G.; Desai, S. P.; Lu, C. C.; Truhlar, D. G.; Penn, R. L. Role of a Modulator in the Synthesis of Phase-Pure NU-1000. *ACS Appl. Mater. Interfaces* **2017**, *9* (45), 39342−39346.
(37) The synthesis of phase-pure NU-1000 was performed according to the literature procedure (see SI and ref 36.) It is worth mentioning that NU-1000 is often contaminated with a polymorph, NU-901. When present as a sizable fraction (∼15−20%), it can typically be detected by close inspection of powder X-ray diffraction data or as a morphologically distinct zone in the center length of microcrystallites. At lower concentrations, its presence can be detected via its contribution to the material's fluorescence—most notably as a spurious addition to the red side of the spectrum.
(38) Hadjiivanov, K. I.; Panayotov, D. A.; Mihaylov, M. Y.; Ivanova, E. Z.; Chakarova, K. K.; Andonova, S. M.; Drenchev, N. L. Power of Infrared and Raman Spectroscopies to Characterize Metal-Organic Frameworks and Investigate Their Interaction with Guest Molecules. *Chem. Rev.* **2020**, DOI: 10.1021/acs.chemrev.0c00487.
(39) Lu, Z.; Liu, J.; Zhang, X.; Liao, Y.; Wang, R.; Zhang, K.; Lyu, J.; Farha, O. K.; Hupp, J. T. Node-Accessible Zirconium MOFs. *J. Am. Chem. Soc.* **2020**, *142* (50), 21110−21121.
(40) The antenna behavior is conceptually similar to the polymer-based amplified quenching.
(41) Thomas, S. W.; Joly, G. D.; Swager, T. M. Chemical Sensors Based on Amplifying Fluorescent Conjugated Polymers. *Chem. Rev.* **2007**, *107* (4), 1339−1386.
(42) Tan, C.; Atas, E.; Müller, J. G.; Pinto, M. R.; Kleiman, V. D.; Schanze, K. S. Amplified Quenching of a Conjugated Polyelectrolyte by Cyanine Dyes. *J. Am. Chem. Soc.* **2004**, *126* (42), 13685−13694.
(43) Förster, T. Zwischenmolekulare Energiewanderung und Fluoreszenz. *Ann. Phys.* **1948**, *437* (1−2), 55−75.
(44) Nield, J.; Redding, K.; Hippler, M. Remodeling of Light-Harvesting Protein Complexes in Chlamydomonas in Response to Environmental Changes. *Eukaryotic Cell* **2004**, *3* (6), 1370−1380.
(45) Mirkovic, T.; Ostroumov, E. E.; Anna, J. M.; van Grondelle, R.; Govindjee; Scholes, G. D. Light Absorption and Energy Transfer in the Antenna Complexes of Photosynthetic Organisms. *Chem. Rev.* **2017**, *117* (2), 249−293.
(46) For simplicity, we limited our analysis of quantum yields, and our resulting assessment of k_e, to the case where a photo-excited linker will be proximal to only one quencher.
(47) Higher loading of DNB (2.8 DNB/Zr_6 node) gives disproportionately shorter fluorescence quenching times (0.01 ns), possibly due to DNB crowding enforcing a more favorable electronic interaction between DNB and the linker. This is further evidence from a charge-transfer band that appears in the diffuse reflectance spectrum at high DNB loading.
(48) Weller, A. Photoinduced Electron Transfer in Solution: Exciplex and Radical Ion Pair Formation Free Enthalpies and their Solvent Dependence. *Z. Phys. Chem.* **1982**, *133* (1), 93.
(49) Gopal, P.; Reddy, T. M.; Reddaiah, K.; Raghu, P.; Narayana, P. V. An electrochemical investigation and reduction mechanism of 3, 5-Dinitrobenzoic acid at a glassy carbon electrode: A voltammetric study. *J. Mol. Liq.* **2013**, *178*, 168−174.
(50) Given the flexible nature of tethering, for both DNB and Fc, it seems likely that RDA spans a range of distances. The DFT-optimized value is used only for the sake of concreteness. Even sizable inaccuracies in R_{DA} are anticipated to yield only small changes in the estimated value of ΔG, as the electrostatic terms in eq 3 are only minor contributors to its value.
(51) Note here, the DFT-optimized geometry of DNB attached to the Zr_6 node suggests that the quencher is tilted toward one of the TBAPy linkers. Note also that single-crystal X-ray structures for various node-appended, substituted benzoates show that these nonstructural ligands engage in monodentate, ester-like binding to a single Zr(IV) ion—a linkage that allows for considerably flexibility (refs 32 and 33).
(52) Bucior, B. J.; Rosen, A. S.; Haranczyk, M.; Yao, Z.; Ziebel, M. E.; Farha, O. K.; Hupp, J. T.; Siepmann, J. I.; Aspuru-Guzik, A.; Snurr, R. Q. Identification Schemes for Metal−Organic Frameworks To Enable Rapid Search and Cheminformatics Analysis. *Cryst. Growth Des.* **2019**, *19* (11), 6682−6697.